UAS-Borne Radar for Autonomous Navigation and Surveillance Applications

Christos Milias, *Student Member, IEEE*, Rasmus B. Andersen, Bilal Muhammad, Jes T. B. Kristensen, Pavlos I. Lazaridis, *Senior Member, IEEE*, Zaharias D. Zaharis, *Senior Member, IEEE*, Albena Mihovska, *Member, IEEE*, and Dan D. S. Hermansen

***Abstract*— The autonomous navigation of UAS requires, among others, detect-and-avoid capability as a prerequisite for enabling wide-ranging applications, including the transportation of goods and people. This article presents the design, implementation, and experimental results of a UAS-borne radar system detecting drones. The applications of the proposed system include not only detect-and-avoid systems for safe and autonomous navigation of unmanned aircraft systems but also airborne surveillance of malicious drones in controlled or restricted airspace for mitigating security and privacy threats. The system performance in terms of maximum detection range is evaluated through field tests. The experimental results show that the proposed UAS-borne radar can detect a DJI Phantom 4 and a DJI Matrice 600 Pro at a maximum distance of 440 and 500 meters, respectively. The article also provides insights into the system implementation and integration aspects, discusses future research direction, and stresses the need for standardization efforts to benchmark the required performance levels for UAS-borne radars.**

***Index Terms*— Autonomous navigation, drone detection, UAS-borne radar.**

I. Introduction

UNMANNED Aircraft Systems (UAS), commonly known as drones, provide the impetus for creating novel business models and services in wide-ranging sectors, such as agriculture, energy, public safety and security, delivery and e-commerce, mobility, and transport, to name a few. The European drones outlook study forecasts the economic impact to be € 14.5 billion annually by 2050 across the value chain of drone products, services, and operations [1]. The potential increase in drone applications across various sectors will have considerable implications for the safe integration and operations of a large volume of drones in very low-level (VLL) airspace, i.e., below 150 meters, and for maintaining the security and privacy of sensitive installations threatened by malicious drones.

The wide-scale commercial operation of drones supported by the UAS Traffic Management (UTM) system requires detect-and-avoid (DAA) capability onboard drones to prevent collision with other participating aircraft and man-made and natural obstacles [2], [3]. The necessity for reliable DAA systems intensifies as the UAS airspace becomes increasingly crowded. Given the ongoing fast-paced development of UTM systems worldwide for unlocking the true potential of drones [4], [5], [6], it is paramount to develop and test the enabling systems and technologies to facilitate the safe navigation of large volumes of drones and also prevent unauthorized or malicious drones from compromising the safety, security, and privacy of sensitive installations.

A. Existing Detection Methods

Radars, lidars, cameras, passive RF (Radio Frequency) sensing, temperature sensors, and acoustic features are among the most popular DAA and UAS detection methods [7]. Lidars are suitable only for short-range applications [8], [9], [10], [11], while video and image detection require line-of-sight and are prone to fog and low light conditions [12], [13], [14]. Sound-based (acoustic) techniques suffer from environmental noise and fail in a noisy urban environment [15], [16]. RF sensors that detect electromagnetic signals are preferred for detecting drones and their controllers. However, these techniques become ineffective in detecting non-cooperative man-made and natural obstacles. Furthermore, in the case of cellular-connected UAS (i.e., drones operated via 4G and 5G networks), RF-based drone detection becomes challenging [17], [18]. Compared to these techniques, radar systems are superior because they offer wide coverage and a long detection range and operate under all-weather conditions at any time of the day [19], [20], [21]. Owing to this, they are an effective and reliable solution that can provide early warnings and enhance situational awareness. Besides detection, target classification is an essential aspect of a radar system. Fortunately, multicopters have a unique micro-Doppler signature due to the rotation of their propellers [22]. This feature can facilitate classification and help distinguish drones from other radar targets such as buildings, terrain, and birds.

Manuscript received 21 July 2022; revised 21 November 2022 and 19 January 2023; accepted 3 March 2023. Date of publication 16 March 2023; date of current version 7 July 2023. This work was supported by the European Union through the Horizon 2020 Marie Skłodowska-Curie Innovative Training Networks Program "MObility and Training fOR beyond 5G Ecosystems (MOTOR5G)" under Grant 861219. The Associate Editor for this article was Y. Li. *(Corresponding author: Christos Milias.)*

Christos Milias, Rasmus B. Andersen, Jes T. B. Kristensen, and Dan D. S. Hermansen are with MyDefence A/S, 9400 Noerresundby, Denmark (e-mail: cm@mydefence.dk).

Bilal Muhammad and Albena Mihovska are with the Department of Business Development and Technology (BTECH), Aarhus University, 8000 Aarhus, Denmark.

Pavlos I. Lazaridis is with the School of Computing and Engineering, University of Huddersfield, HD1 3DH Huddersfield, U.K.

Zaharias D. Zaharis is with the School of Electrical and Computer Engineering, Aristotle University of Thessaloniki, 54124 Thessaloniki, Greece.

Digital Object Identifier 10.1109/TITS.2023.3254582

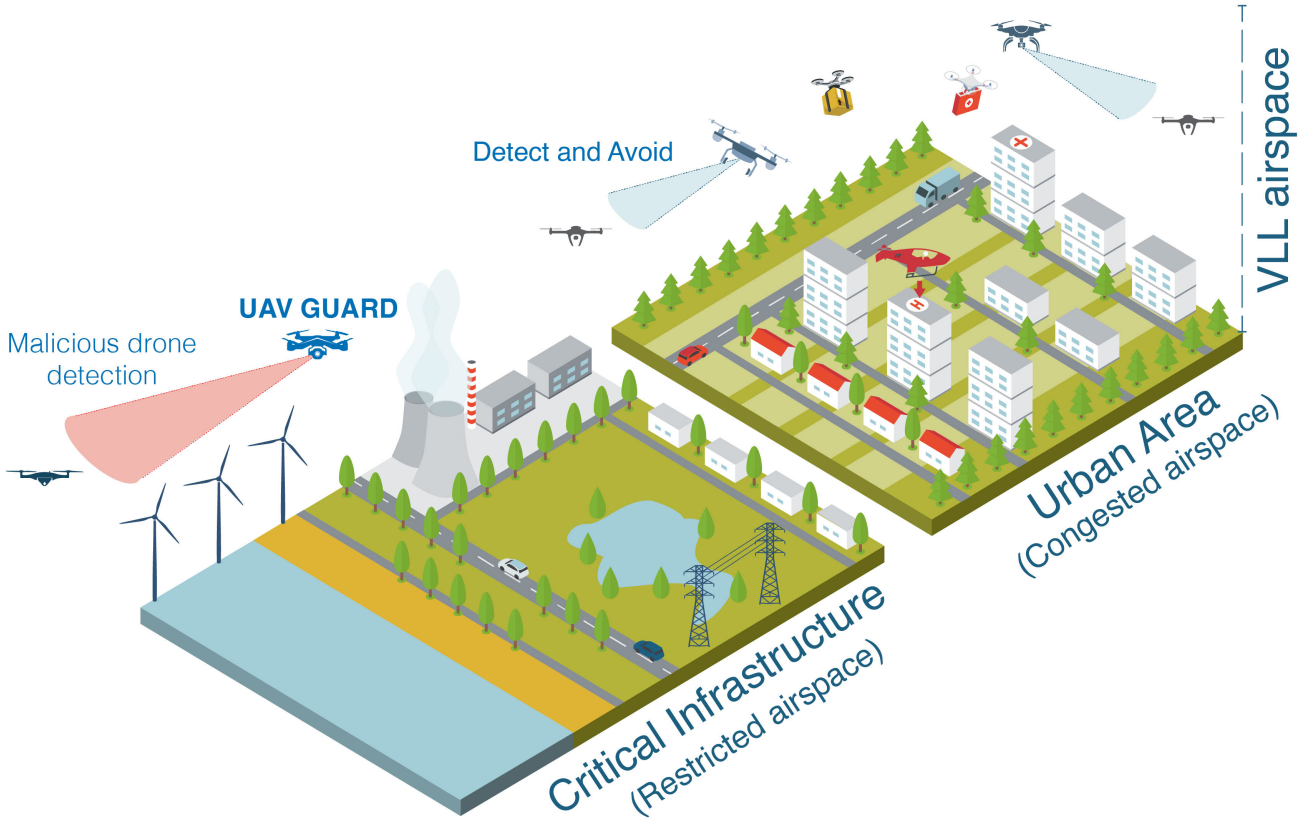

Fig. 1. Illustration of UAS-borne radars monitoring restricted airspace and supporting the safe operation of drones in congested airspace.

Regarding radar types, ground-based radars are typically placed in proximity to critical infrastructures such as airports, power plants, and sensitive public buildings and installations. Their static setup and position limit their detection ability to a specific geographic area. In addition, potential threats can easily hide behind large surfaces and objects like buildings, where they become invisible to the radar. Mobile radars mounted on vehicles such as cars and trucks are a solution to this issue. These radars leverage their mobility to offer additional freedom, which arises from the fact that they are flexible and can be deployed anywhere, depending on application requirements.

Recently, there has been an increasing trend in mounting various sensors or communication equipment on drones, commonly referred to as UAS-borne systems. These configurations can offer significant advantages because they exploit the increased mobility and high altitude of UAS, which are unique characteristics of these vehicles. For example, UAV-borne radars for vital sign detection are presented in [23]. The theoretical principles for a cognitive detect-avoid radar with chaotic waveforms for autonomous UAV navigation applications are presented in [24]. A "UAVs to monitor UAVs" approach adopting UAV dynamic radar networks is proposed in [25]. However, the literature cannot find practical implementations or comprehensive discussions regarding the requirements and challenges for UAS-borne radars in DAA and surveillance applications.

B. Proposed Method and Contribution

In this paper, a UAS-borne radar platform capable of detecting drones is designed and experimentally demonstrated. The proposed solution contributes to the ongoing research and development efforts for enabling drones to detect and avoid various obstacles and other participating aircraft in the VLL airspace. This is necessary for the accomplishment of safe and autonomous navigation. Furthermore, it enables airspace surveillance applications and drone detection in restricted or controlled airspace (i.e., above or in proximity to critical infrastructure), as depicted in Fig. 1, and has the following advantages:

- it enables safe and autonomous navigation of drones in all weather and lighting conditions.
- it is flexible and can be deployed anywhere above land, rugged terrain, sea and oceans, secluded and emergency areas, and on critical infrastructures.
- it can effectively track malicious drones and enable the long-range detection of drones that fly at different altitudes or between buildings in urban areas.
- it experiences favorable wireless propagation conditions with reduced ground clutter, fewer obstacles, and an increased line-of-sight probability, improving detection performance.

The contribution of this work is twofold: This paper is the first to theoretically analyze all the aspects and subsystems of

TABLE I
COMPARISON OF THE PROPOSED UAV-BORNE RADAR WITH PREVIOUSLY REPORTED UAS-BORNE SENSORS FOR DRONE DETECTION

Reference	Sensor	Range	Accuracy	Target parameters	External Conditions	Processing requirements	Power requirements	Cost	Size
[10]	Lidar	Low (70 m)	High	3	High influence	High	Moderate	Moderate	Small
[11]	Lidar	Low (15 m)	High	3	High influence	High	Low	Moderate	Small
[13]	Camera	Low (35 m)	Low	3	High influence	High	Low	Low	Small
[14]	Camera	Low (8 m)	High	3	High influence	High	Low	Low	Small
[26]	X-band Radar	Low (60 m)	Moderate	1	No influence	Low	Moderate	Moderate	Medium
[27]	mm-wave Radar	Low (-)	Low	3	Moderate influence	Moderate	Moderate	Moderate	Small
Proposed	X-band Radar	High (500 m)	High	4	No influence	Low	High	Moderate	Large

a UAS-borne radar. The implications of integrating radar and a drone were previously unexplored, and the unique interactions, characteristics, and challenges of this combination have not been investigated elsewhere. For example, an X-band UAV-borne radar is reported in [26], but key design and system performance considerations, such as implementation concerns, antenna design, accuracy, resolution, target detection, and classification are not given sufficient or any attention at all. The same applies for reference [27], where the proposed radar is also prone to external conditions because it operates at mm-wave frequencies. On the contrary, this paper presents an end-to-end radar solution. For example, the antenna design and signal processing are tailored toward this particular radar application. Furthermore, a comprehensive discussion is included to highlight the remaining challenges and provide future research directions that will ultimately allow for the adoption of UAS-borne radars in intelligent transportation systems. In other words, this paper aims to pave the way towards reliable and effective DAA and security UAS-borne radars and become a point of reference for researchers and practitioners in the field who are interested both in the fundamental theory and practical aspects of these systems. Regarding the content, the main focus of this research is to achieve long-range, accurate, reliable, and uninterrupted drone detection; hence, great emphasis is given to the practical challenges and the experimental setup. Nevertheless, an innovative theoretical radar system and processing framework are also proposed to achieve high performance with relatively low-cost and low complexity. As a result, the implementation process is significantly simplified, and the system's applicability becomes more feasible without sacrificing the radar's detection performance and robustness.

Secondly, the results presented in this work are significantly superior in terms of detection range (ten times higher compared to previous related works), accuracy, and flight time. In fact, the proposed radar provides the highest drone detection range ever reported for a UAS-borne sensor in the literature (both passive and active) and is thus the most promising one. Compared to prior art such as sound-based techniques, lidars [10], [11], and camera/video-based detection schemes [13], [14], the proposed radar is not dependent on external or environmental factors such as weather conditions, background noise and time of day. Hence, it is way more reliable and robust. Moreover, extremely high accuracy allows for the simultaneous estimation of many target parameters, such as range, velocity, height, and direction. It is also notable that this can be achieved with relatively low processing and execution time requirements compared to its lidar and camera counterparts which need considerable computational effort.

To further support these claims and highlight the contribution of this work, Table I provides an insightful comparison between the proposed UAS-borne radar, previously reported radars, and other detection methods reported in the literature. The main disadvantage of the reported solution is the somewhat increased power requirements and the relatively large form factor due to the not negligible size of the antennas and electronic equipment.

To sum up, the innovative elements of this work are as follows:

- It responds to recent calls from studies focusing on drone detection [7], [8], [9], [10], [11], [12], [13], [14], [15], [16], [17], [18], [19], [20], [21], [22], [23], [24], [25], [26], [27], and introduces a fundamentally different approach by installing a radar onto a UAV.
- It addresses the unsolved research challenges raised by recent publications (e.g., [25]), and extends and complements the findings of this work by presenting a physical prototype, thus bridging the gap between simulations and real-world implementation.
- It proposes a method superior to related works both qualitatively and quantitatively, as seen in Table I.
- It reports experimental results for the first time in the literature, such as the impact of the radar-carrying drone's propellers, the effect of transmitter-receiver coupling, estimation for the range and speed accuracy, and detection performance.

Based on the above, the contribution of this paper to the existing body of knowledge and its innovative approach to a difficult research problem is demonstrated.

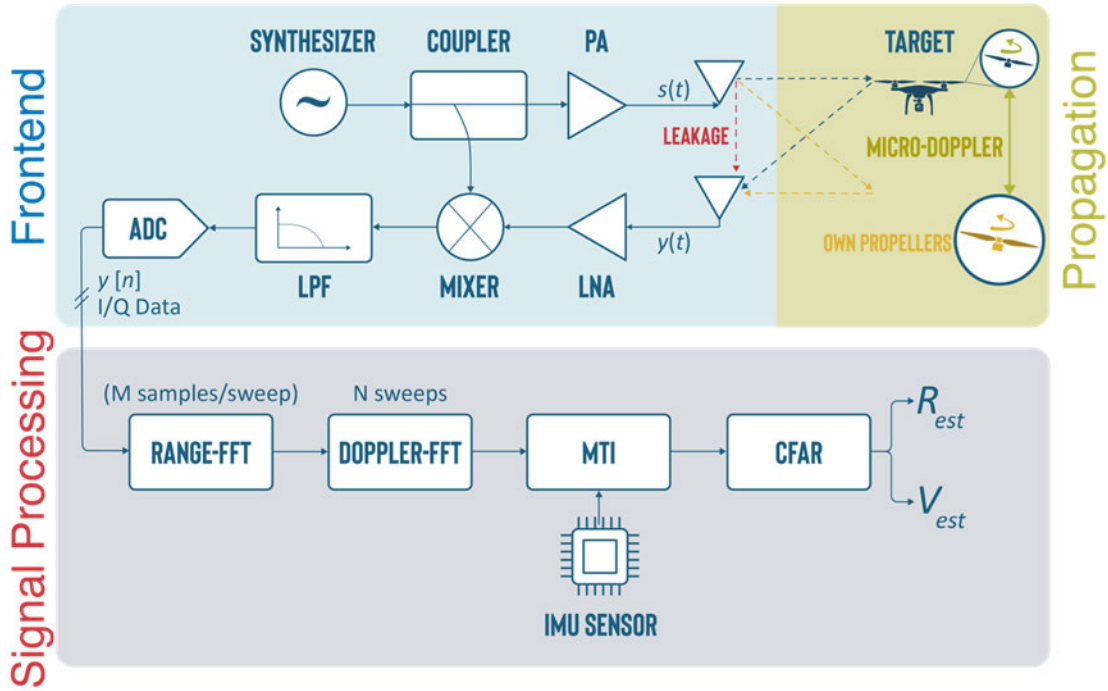

Fig. 2. General overview of the UAS-borne radar system, including the propagation channel, frontend, and signal processing subsystems.

C. Organization

This paper is organized as follows: the fundamental theory concerning radar principles and important system factors is provided in Section II. Considering the theoretical considerations, the implementation description follows in Section III. This includes the radar's antennas, their relative placement to achieve sufficient transmitter-receiver isolation, and the integration of all the required electronic, sensing, and communication equipment onto the UAS's body. The respective practical challenges and limitations are pointed out and described in detail. Subsequently, the experimental results are reported in Section IV. Two different drone targets were utilized and successfully detected during the experiments: a DJI Phantom 4 and a DJI Matrice 600 (M600) Pro. A comprehensive radar signal processing analysis is carried out to examine the key parameters and evaluate the system's performance. Interesting observations, such as the effect of the radar-carrying drone's propellers, are presented for the first time. Based on the measurements, it is concluded that the proposed radar platform can detect a Phantom 4 and an M600 Pro at a maximum range of 440 and 500 meters, respectively. Section V discusses the future challenges and trends for UAS-borne radars, while Section VI draws some conclusions.

II. Radar System

The radar system considered in this article has a frequency-modulated continuous-wave (FMCW) architecture and is based on the fast-chirp modulation described in [28]. FMCW radars are popular due to their adequate range resolution and the fact that they have no blind spots, as is the case with pulse radars. Hence, they are capable of short-range detection. However, they are more susceptible to ground reflections and suffer from reduced dynamic range due to the strong coupling between the transmitter and receiver. A general and concise overview of the UAS-borne radar architecture, including its hardware, signal processing, and propagation subsystems, is shown in Fig. 2.

A. Hardware(Frontend)

The frontend comprises a frequency synthesizer, which produces the desired periodic FMCW waveform transmitted by the radar's transmitting antenna after being amplified by a power amplifier (PA). The transmitted FMCW waveform $s(t)$ is mathematically expressed as:

$$s(t) = \sqrt{2P_t}cos\left[2\pi\left(f_0 + f(t)\right)t\right], \quad 0 < t < T_{sw} \tag{1a}$$

$$f(t) = f_1 + kt \tag{1b}$$

Here, f_0 is the carrier frequency, $f(t)$ is the linear frequency sweep with a minimum value of f_1 and maximum value of f_2, T_{sw} is the sweep time, P_t is the transmitted power, while the bandwidth is given by: $BW = f_2 - f_1$. The slope of the linear sweep is $k = BW/T_{sw}$. The range resolution ΔR depends on the bandwidth, while the maximum unambiguous range R_{max} is a function of the sweep time:

$$\Delta R = \frac{c}{2\,BW} \tag{2a}$$

$$R_{max} = \frac{c\,T_{sw}}{2} \tag{2b}$$

A small portion of this signal is fed into the receiver's (Rx) mixer with the help of a coupler placed before the PA. A low-noise amplifier (LNA) at the receiver side boosts the received signal y(t), which is then fed into a quadrature mixer. The mixer's output, commonly known as a beat signal, is passed

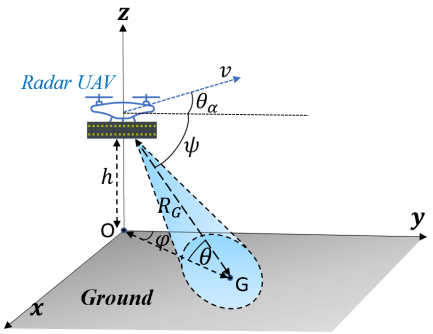

Fig. 3. UAS-borne radar antenna array above ground.

through an LPF (low-pass filter) that removes all the undesired inter-modulation products. Thus, the signal is immediately sampled by an Analog-to-Digital Converter (ADC) and passed to the digital signal processing domain in the form of In-phase and Quadrature (I/Q) data.

In most cases, an additional high-pass filter with a transfer function denoted by $H(f)$, is placed before the ADC to preserve a reasonable dynamic range (dynamic range compression). This is required in FMCW radars because there is a direct signal leakage (from the transmitter to the receiver) which is several orders of magnitude higher than the weak target echo. A high-pass filter can suppress the leakage (which occupies mainly the DC and low beat frequencies since there is a negligible time delay) and restore the dynamic range.

B. Propagation

The transmitter's (Tx) high-gain antenna illuminates the environment. The emitted waves propagate toward the surrounding objects and targets, where they get reflected and diffracted. Subsequently, a part of the power returns, and the receiving antenna captures it. Apart from the target's echo $y_T(t)$, there are three other main contributors to the total received signal: a) the direct signal leakage $y_L(t)$ from the Tx to the Rx antenna due to the mutual coupling between them b) the strong ground returns that produce an overall contribution (ground clutter) which is denoted by the $y_c(t)$ and c) the time-varying reflections $y_p(t)$ caused by the UAS's propellers (the propellers of the drone that carries the radar) that are placed in proximity to the radar's antennas and create a modulated backscattered signal due to their rotation. Hence, the total received signal can be written as:

$$y(t) = y_T(t) + y_L(t) + y_C(t) + y_p(t) \tag{3}$$

While y_T, y_C, and y_L are signal components found in all radars (e.g., automotive, ground-based), y_p is a unique component only observed in UAS-borne radars carried by propeller-based drones.

C. Signal Processing

Signal processing techniques are necessary to extract the desired signal's $y_T(t)$ information while suppressing the influence of the undesired components. Fast Fourier Transform (FFT) is initially applied to a set of M complex (I/Q) samples of the same sweep return. This FFT is commonly referred to as Range-FFT. Subsequently, a group of N Range-FFTs is combined, and the so-called Doppler-FFT is applied along the orthogonal dimension (i.e., sweep dimension). The result is the Range-Doppler map, an M/2 x N image containing range and speed information about the illuminated environment. The Range-Doppler map is then exploited for detecting and estimating the target's range and speed relative to the radar.

To retrieve this information, the constant false alarm rate (CFAR) algorithm and, more specifically, its cell-averaging variation is utilized for detection [29]. This algorithm estimates the background noise level by calculating the average power of neighboring cells, known as training cells that surround the CUT (cell under test). Guard cells (i.e., cells whose power is not used for noise estimation) are placed adjacent to the CUT to avoid strong signal components from leaking into the training cell since this would unfavourably affect the noise estimate. Depending on the desired probability of a false alarm and the noise power estimation, an appropriate threshold is calculated and compared to the power of the CUT to determine whether there is detection or not. However, some Range-Doppler cells, whose high power originates from strong reflections (clutter) due to the ground or other stationary objects (e.g., buildings), exceed their respective detection threshold.

These false detections can be ruled out by a moving target indicator (MTI) that differentiates the moving targets from the stationary background [30]. Hence, the Range-Doppler cells with zero speed (or close to zero) are excluded from detection. It is relatively straightforward to apply the MTI when considering a stationary radar. Unfortunately, this is not the case for moving radars such as airborne platforms or the UAS-borne system reported here. This is because the radar is not stationary relative to the ground and the surrounding buildings, and thus the latter appear as moving targets on the Range-Doppler map. Considering Fig. 3, which depicts the UAS-borne radar system equipped with a 2D antenna array, the Doppler shift f_d of the reflection due to ground point G is given by the well-known equation [31]:

$$\begin{aligned} f_d &= \frac{2v}{\lambda}\cos(\phi+\theta_\alpha)\cos\theta \\ &= \frac{2v}{\lambda}\left(\cos\psi\cos\theta_\alpha - \sin\theta_\alpha\sqrt{1-(\frac{h}{R_G})^2-\cos^2\psi}\right) \end{aligned} \tag{4}$$

where the x-axis is perpendicular to the array axis, v is the UAV's speed, h is its altitude, R_G is the distance to the ground point G, and θ_α is the angle between the y-axis and the flight direction. Moreover, ϕ, θ, and ψ denote the azimuth, elevation, and conical angles, respectively. This equation shows the range and angular dependency of the Doppler frequency for moving radars. For example, this relationship is a parabolic function in the case of a forward-looking, forward-moving radar. An onboard IMU (Inertial Measurement Unit) sensor that provides speed and orientation information can be utilized to suppress this effect. The IMU data can be used to compensate for the UAS's movement and ultimately avoid false detections

caused by the stationary clutter. In addition, it allows for the correct estimation of the target's speed.

D. Theoretical Analysis and Practical Challenges

From the previous subsections, it becomes obvious that the design of a radar system, particularly a UAS-borne, involves several design factors and disciplines ranging from electromagnetics to signal processing and aerodynamics. Meanwhile, cost and application requirements should also be taken into account. This subsection uses simple yet effective design rules to gain better insight into the radar's performance, emphasizing its limitations and key trade-offs. These guidelines are then used to derive the values of important system parameters, such as the processing and antenna gain, to meet specific requirements like maximum detection range, velocity, angular resolution, computational time, and complexity. A general system architecture tailored towards UAS-borne systems is proposed. Towards this end, the following theoretical analysis is a mixture of standard radar theory and advanced modifications to account for the special case of UAS-borne radars. Practical considerations are involved as well, to appropriately facilitate the implementation process with prior knowledge extracted from the applied theoretical analysis.

One of the most important factors determining the radar's detection performance is the signal-to-noise ratio (SNR). The SNR at the receiver after signal processing is given by the following equation:

$$SNR_{out} = \frac{P_r}{P_N} = \frac{P_t\, G^2\, \lambda^2 \sigma\, G_p}{(4\pi)^3\, R^4\, L\, k B_e T_0\, NF} \tag{5}$$

where P_r is the received power after signal processing, P_N is the noise power, $P_t = 10$ Watts is the transmitted power, B_e is the effective bandwidth (i.e. FFT bandwidth in this case), G is the antenna gain (assuming same gain for the Tx and Rx antennas), $\lambda = 3$ cm is the wavelength at the carrier frequency of $f_0 = 10$ GHz, σ is the monostatic radar cross-section (RCS) of the target (typically between 0.02 and 0.1 m^2 for the drone targets considered here [32], [33]), R is the distance to the target, k is the Boltzmann constant, $T_0 = 290$ is the temperature in Kelvins, $NF = 4$ dB is the receiver's noise figure, and $G_p = N$ is the processing gain due to the coherent integration of N sweep returns. A parameter L, ranging between 2 and 5 dBs, is also included to model other types of losses such as atmospheric attenuation, polarization mismatch, etc. Some of the above parameters, such as the transmitted power, carrier frequency, waveform bandwidth, and receiver noise figure, are predetermined by the radar hardware that will be utilized in practice and thus cannot be changed. Hence, the main design parameters that have a significant impact on the SNR and can be configured here are the processing gain G_p, and antenna gain G.

The processing gain can be enhanced by integrating more sweep returns N and consequently performing more computations and FFTs. As a result, it leads to a trade-off between achieving a higher SNR and reducing the computational and target observation time, directly affecting the update rate. Given that UAVs are high-mobility platforms, it is essential to maintain a high update rate regarding their position and velocity. Another important implication of increasing the number of FFTs is the improvement of the doppler/speed resolution, as the following equation reveals:

$$\Delta v = \frac{c}{2 f_0 N T_{sw}} \tag{6}$$

Of course, more memory storage per cycle (Mem. Storage = NML_{bit} bits, where L_{bit} is the number of bits of the ADC) is required for better resolution. It is decided to set N equal to 128, which is a reasonable compromise between the processing gain and the memory storage and computation time per cycle. This choice is particularly suitable for DAA applications where timely detection and fast update rates are of greater importance than the maximum detection range. Given this value, the cycle duration lasts for 38.4 ms. Given that commercial drones have a maximum speed of about 25 m/s, their maximum displacement per cycle does not exceed 1 m (25*0.0384 = 0.96), which is a sufficient value for most applications and avoids the problem of range migration. Moreover, this choice provides an adequate speed resolution of $\Delta v = 0.39$ m/s (or 1.4 km/h).

As far as the antenna gain is concerned, it can be increased at the cost of a larger antenna aperture (i.e., $G \propto \frac{4\pi D}{\lambda^2}$, where D denotes the antenna aperture). On the one hand, the deployment of large antennas can be detrimental to the flight efficiency of UAVs as it potentially degrades their aerodynamic performance and increases the weight of the overall payload. Furthermore, phased arrays comprising a large number of antennas require a considerable amount of phase shifters, amplifiers, and other components. Thus, the overall cost and power consumption scale up linearly with the number of elements. On the other hand, the angular resolution of the radar is improved since it is proportional to the antenna half-power beamwidth ($HPBW$) and to the antenna aperture ($HPBW \propto \lambda/D$). For a successful detection by the CFAR algorithm, the SNR should typically exceed 13 dB ($SNR^{dB}_{min} \geq 13$) assuming a typical probability of detection and false alarm: ($P_D \geq 0.9$, $P_{fa} \leq 10^{-6}$). Substituting all parameter values to Eq. (5), an antenna gain higher than 15 dBi is sufficient to provide a maximum detection range above 400 m.

Since UAVs are highly dynamic vehicles moving in 3D space, the proposed radar must be capable of estimating the target's direction (azimuth bearing) and its altitude. To achieve this, the antenna array architecture of Fig. 4 is adopted here. The transmitter's array (Tx) is composed of $N_x \times N_y$ elements

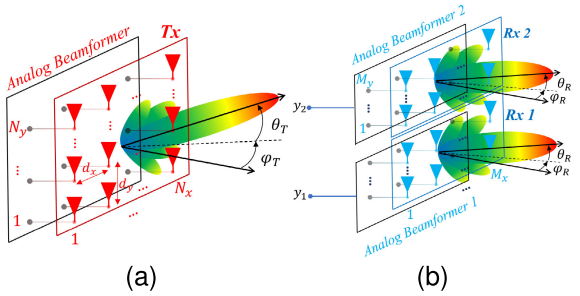

Fig. 4. Conceptual illustration of (a) transmitter antenna array and (b) hybrid receive antenna array.

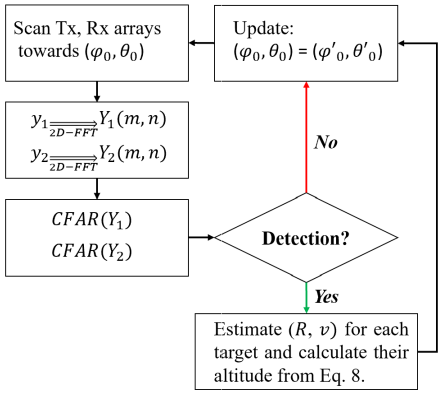

Fig. 5. Flow chart of the processing and execution steps for the detection scheme adopted here.

and utilizes exclusively analog beamsteering to steer its beam towards the azimuth and elevation angles of ϕ_T, θ_T. Analog beamsteering is preferred here over its digital counterpart, providing a better cost-performance ratio. The receiver comprises two antenna arrays, Rx 1 and Rx 2, each consisting of $M_x \times M_y$ elements and connected to its dedicated analog beamforming unit. To estimate the target's azimuth bearing, the main beam of the two subarrays Rx 1 and 2 is steered concurrently with the transmitter's beam: $\phi_R = \phi_T, \theta_R = \theta_T$). Subsequently, if a target is detected towards this particular direction, its elevation angle can be estimated from the phase difference (due to time delay) between the Rx 1 and Rx 2 baseband signals $y_1(t)$ and $y_2(t)$. To this end, the transformation of the discrete-time signal y consisting of $M \times N$ samples to its corresponding range-Doppler response (i.e., after the 2D-FFT), is denoted by $Y(m,n) \in C$, where $m = 1, \ldots, M/2$, and $n = 1, \ldots, N$. The elevation angle of a target detected at the range bin m_0, Doppler bin n_0, is given by:

$$\theta^\star = \arcsin\left(\lambda \frac{\angle Y_2(m_0, n_0) - \angle Y_1(m_0, n_0)}{2\pi d_{Rx}}\right) \tag{7}$$

where d_{Rx} is the spacing between the phase centers of Rx 1 and Rx 2. Then, the target's altitude can be estimated as:

$$h^\star = h + R^\star \sin\theta^\star \tag{8}$$

Here, $R^\star$ is the target's estimated range that the radar and h is the UAV-borne radar's own altitude, which is known either through GPS or barometer data. The flow chart of the proposed architecture is presented in Fig. 5. Moreover, the detection and parameter estimation of multiple targets is possible, given that the targets are separated at least in one dimension (i.e. range, velocity, or azimuth bearing). In fact, this method is the most low-cost (only two Rx channels) and computationally efficient way for estimating all four target parameters, as it requires only two 2D-FFT transforms and two CFAR executions per cycle. As a result, it is extremely suitable for UAV platform where space and power consumption constraints dictate the system architecture.

It should be pointed out that this analysis is a theoretical one, and the actual radar performance may be different in practice as it highly depends on some other unpredictable factors such as propagation conditions, antenna coupling, system nonlinearities [34], and target swerling [35]. Nevertheless, it is still a useful approximation that facilitates the design process and assists in calculating or predicting important system parameters.

III. Implementation

A. Radar and UAS Platforms

The radar platform used in this work is provided by MyDefence A/S. It operates at the center frequency of 10.05 GHz and employs the previously described FMCW architecture with a transmit power of 10 Watts (RMS) and a bandwidth of 45 MHz, corresponding to a range resolution of $\Delta R = 3.9$ meters. All the electronic components, including the power supply, RF, and processing PCBs (printed circuit boards) and the required cables, are enclosed inside a box with $18 \times 18 \times 18$ cm dimensions. This enclosure consists partly of aluminum and partly of lightweight 3D-printed parts. The overall system consumes a total power of 40 Watts and requires 40 Volts DC as supply voltage. A heatsink is attached to the aluminum plate of the enclosure to dissipate the heat generated by the circuits and regulate the temperature. Two RF SMA connectors are also placed for connecting the Tx and Rx antennas. Moreover, an ethernet cable transfers commands and data to and from the radar system and a laptop. This way, the radar can be configured and controlled from an external device and transfer the captured data. It should be noted that this radar platform is utilized here exclusively for raw IQ data recordings, and no processing takes place in it.

The UAS platform, Alta X, developed by Freefly Integrations [36], is chosen for the experimental setup. It has an unfolded diameter of 1.145 m and features four carbon fiber propellers, 84×23 cm each. It can fly for 50 minutes without a payload and approximately 20 minutes with a 10 kg payload. The Alta X cargo landing gear, an expandable and adaptable platform that integrates custom payloads, is attached to the drone body. A cargo tray kit is added to the landing gear to support the payload. The tray is made of carbon fiber with vertical stiffeners to ensure good performance even with heavy loads. The tray features slots and tie-down points that allow attaching the payload securely. This configuration facilitates the mounting of the radar platform onto the drone and provides excellent flexibility.

B. Antennas

Typically, high-gain antennas with narrow beams are utilized in radar systems to provide a long detection range and fine angular resolution. Radar scanning is achieved by either mechanical rotation of the antennas or by electronic means via the deployment of phased arrays. The antenna aperture's physical rotation offers 360° coverage, low cost, and low complexity. On the other hand, electronic scanning provides a quick response but is limited to a specific angular sector. Hence, a hybrid combination of the two methods yields the best scanning performance with advanced flexibility and moderate cost. As far as UAS-borne antennas are concerned, two main parameters shall be considered. First, an aerodynamic

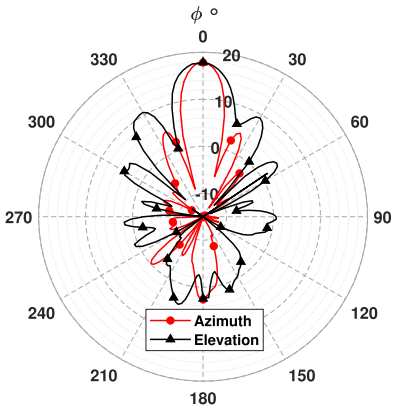

Fig. 6. Measured azimuth and elevation radiation patterns of the radar antennas.

shape that exhibits low drag is desired for seamless integration with the UAS structure without mitigating its flight efficiency. Therefore, airfoil and ogive-shaped antennas are ideal for this application. In addition, lightweight antenna structures are necessary for maximizing flight time.

To satisfy these requirements and by considering the design considerations of Sec. II-D, two 8-element arrays (one for Tx and one for Rx) consisting of printed Yagi-Uda antennas arranged in a 4×2 configuration are utilized (i.e. $M_x = N_x = 4$, $N_y = 2$, $M_y = 1$.) This antenna array was designed by the authors as part of the same research project and provides the required gain and scanning range with a reasonable amount of array elements. It operates at the desired center frequency of 10.05 GHz and offers a forward realized gain of 17.5 dBi. Its beam can be steered from $-25°$ to $+25°$ and from $-18°$ to $+18°$ in azimuth and elevation, respectively. The maximum gain variation during scanning is 1 dB, while the corresponding azimuth side lobes are below -10 dB. The radiation pattern of the antenna array pointing towards the boresight direction ($\phi = \theta = 0$) in azimuth and elevation plane are shown in Fig. 6.

Furthermore, this type of antenna provides pure horizontal polarization, which is desired since UASs exhibit higher H-polarization monostatic RCS (Radar Cross Section) compared to the V-polarization RCS. Besides height estimation, there are two more reasons for choosing a 4×2 (i.e., 2D array) configuration: i) It is crucial to perform beamsteering in the elevation plane to compensate for the cases where the UAS points slightly downwards/upwards when it moves forward/backward (i.e., non-zero pitch), and also for the detection of targets that fly at different altitudes ii) it provides a narrow beam in the elevation plane (compared to 1D arrays) and thus the reflections from the ground underneath the radar have less impact on the received signal. Hence, the signal-to-clutter ratio (SCR) is improved.

To protect the exposed antenna array, it is placed inside a 3D-printed radome with a parabolic nose cone profile. This shape exhibits reduced aerodynamic drag compared to planar antenna apertures. Finally, the total weight of the radome and the antenna boards is negligible, as no heavy structures are utilized. It should be pointed out that for the sake of the cost of the measurement campaign reported here, beamsteering is not demonstrated in practice as it requires additional expensive circuitry (e.g., RF phase shifters for analog beamforming or several receiver chains for digital beamforming), and the existing radar platform does not support this functionality. Hence, the antenna elements of the array are fed directly by standard power dividers that provide equal amplitude and phase to all eight elements of the 4×2 array (uniform distribution). This results in a fixed array beam. Of course, the dividers introduce additional loss to the system (around 3 dB at 10.05 GHz). Nevertheless, this loss can be considered and compensated when estimating the maximum detection range.

C. Tx-Rx Isolation

The sensitivity and dynamic range of FMCW radars are severely affected by the phase noise included in the transmitter's signal, which leaks into the receiver [37], [38]. This leakage is usually of considerable magnitude compared to the target's echo; thus, the SNR is significantly decreased. To achieve the required isolation, the Tx and Rx antennas must be placed at an adequate distance from each other. The noise level is measured for several distances between the two antenna arrays (ranging from 20 cm up to 80 cm) to find the proper placement that yields acceptable isolation. During this investigation, the antennas are placed outdoors and mounted on the Alta X at 1.5 meters above the ground. For each distance, the radar illuminates the same stationary environment that does not include any targets, and the respective IQ data are recorded. As a result, the received signal consists mainly of clutter returns and leakage noise, which must be estimated. This is achieved by constructing the Range-Doppler map and averaging the power of the bins over the Doppler domain. The center bins, which correspond to ground clutter returns (i.e., for speeds from -0.5 to $+0.5$ m/s), are excluded from this calculation to focus on the contribution of the leakage. In this manner, a noise power vs. range curve for each Tx-Rx antenna distance is created. As expected, the noise floor decreases as the distance between the Tx and Rx antennas increases. Based on these measurements, it is decided to place the antennas at 70 cm from each other since increasing the separation more than that has a negligible effect on the radar's sensitivity and dynamic range.

D. Final Setup

The final step includes the integration of the radar and drone platforms, as well as the configuration of the required equipment for onboard control, communications, and data storage. A mini laptop (Lenovo Yoga 3) with an average battery life of 30 minutes and a compact design (1.6 kg, 14 inches) is utilized for this purpose. A 4G USB dongle (Huawei E3372 USB modem) is connected to the laptop to provide internet connectivity while flying. Furthermore, the laptop computer is connected to the radar platform via a USB Ethernet adapter. This way, control commands can be sent from the mini laptop to the radar, transferring the recorded IQ data to the laptop for storage. The commercially available TeamViewer software

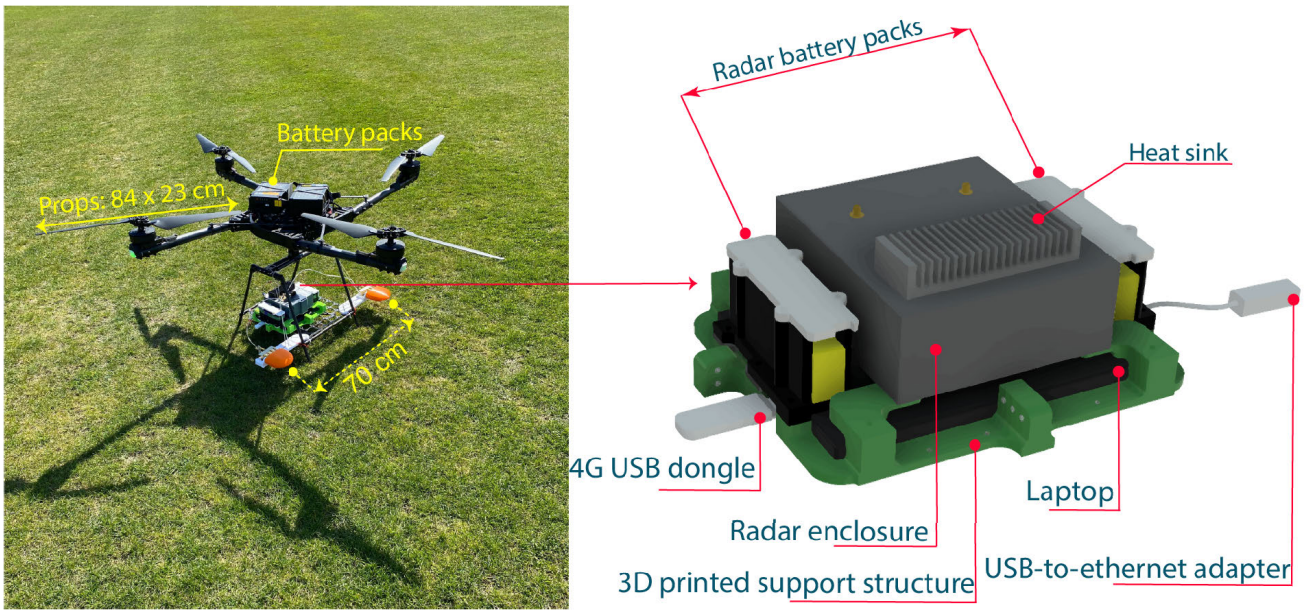

Fig. 7. Experimental setup of the UAS-borne radar.

is used to access the mini laptop remotely from a ground-based computer. Hence, the radar can be controlled remotely seamlessly while the data are stored onboard. To power the radar, two 20 Volt batteries are connected in series. The final setup is shown in Fig. 7. For mounting this equipment on the cargo tray kit, a 3D-printed structure (green color) is designed and attached to the tray with screws. It secures the laptop computer firmly and provides the mechanical support required during flights. The radar enclosure is placed precisely above the laptop, which is mechanically connected to the 3D-printed structure through metallic rods. A gap of 1 cm is left between them for proper air circulation. Two small boxes (black color with white top cover) are also printed to accommodate the radar batteries (yellow color). The antennas (orange color) are secured by two wing-shaped structures (white color), which are screwed onto the tray kit and provide the required spacing between them (70 cm) for proper isolation. Two RF cables with a length of 60 cm and a loss of 1 dB are used to connect the antennas with the input and output of the radar.

IV. Experimental Results

A. Clutter and Impact of Own Propellers

This section discusses the experimental findings related to the UAS-borne radar setup. The impact of the ground clutter and the rotation of the drone's propellers on the received signal are qualitatively analyzed by observing the range-Doppler spectrum of the response. Subsequently, the drone detection performance is quantitatively examined by extrapolating the experimental data to estimate the maximum detection range and evaluate the range and speed accuracy of the system. Given that two different targets are continuously detected with high accuracy and reliability, the robustness of the radar sensor is validated.

The first measurement was focused on the ground clutter effect. For this reason, Alta X was flying forward toward the direction of the antenna's main beam (forward-looking - forward-moving case) at a height of 20 meters above the ground. The respective IQ samples ($M = 1024$ per sweep) of the illuminated environment were recorded, and the corresponding range-Doppler map constructed through the integration of $N = 1024$ sweep returns is presented in Fig. 8a. As shown, the range-Doppler profile of the ground reflections follows the expected parabolic profile predicted by the theoretical calculations. It should be noted that a Dolph-Chebyshev window with a side lobe level of -90 dB is applied to the samples before both Range- and Doppler-FFTs.

To investigate the impact of the radar-carrying drone's propellers, Alta X was left hovering (zero velocity) during the recordings. The respective range-Doppler map ($M = N = 1024$) is shown in Fig. 8b. The reflections from Alta X's propellers significantly impact the received signal and span across the whole speed dimension. It can be observed that the negative Doppler bins have a larger magnitude than their positive counterparts. This happens because the propellers were more visible to the radar antennas when approaching than when moving away. It should be noted that this phenomenon is unique to this type of radar, and it is a challenging problem as it can mask targets whose echo occupies the same range as Doppler bins.

B. Drone Detection

Two different drones were used as targets during the experiments. The first is a DJI Phantom 4 with four propellers, while the second is a DJI M600 Pro with six propellers. All drones had GPS sensors onboard to provide accurate range and speed information concerning the radar. The GPS data can then be compared with the radar's post-process estimations. The experiments were performed over relatively flat terrain under good weather conditions. It should be stressed that since radars utilise radio frequency (RF) electromagnetic waves to sense

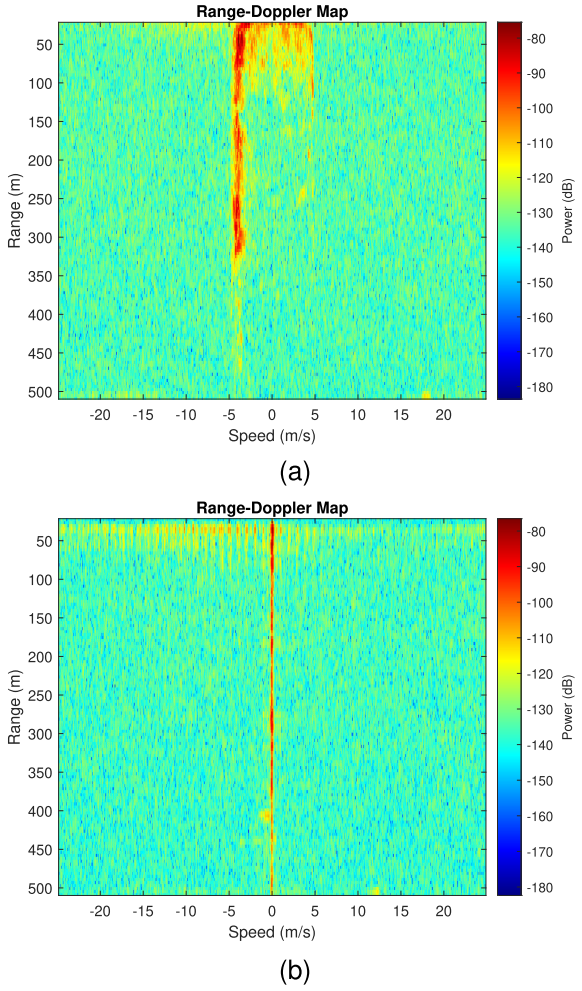

Fig. 8. (a) Range-Doppler Map while Alta X was moving forward. (b) Snapshot of the Range-Doppler Map while Alta X was hovering.

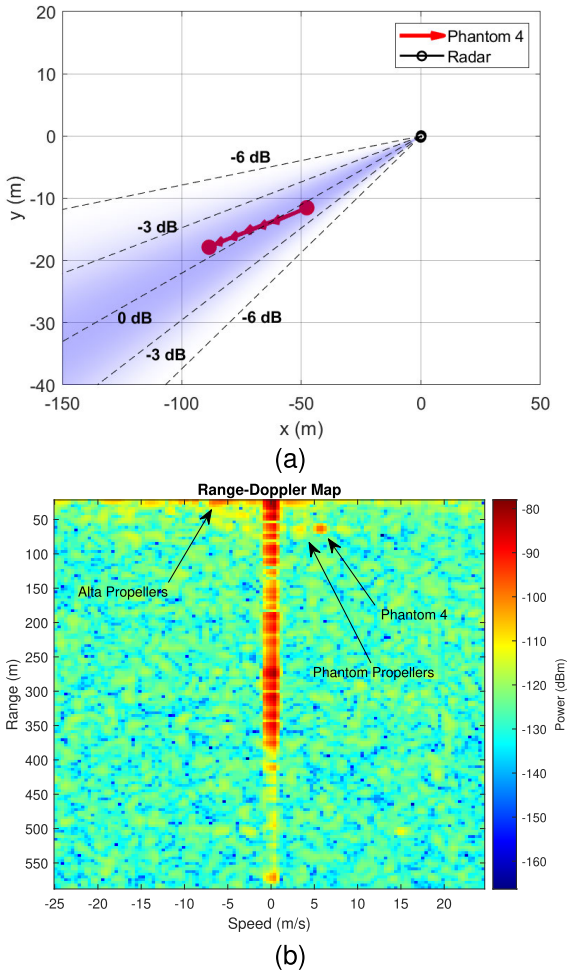

Fig. 9. (a) The GPS trajectory of the DJI Phantom 4 during the experimental IQ recordings. (b) Snapshot of the Range-Doppler map constructed from DJI Phantom 4 measurements.

the environment, their performance is not affected by light or weather conditions (or is negligibly affected due to attenuation), as is the case for wireless communication systems. Hence, it follows that the measurements of this research work are completely independent of external factors, and therefore, they are valid and can be generalized for all scenarios. As a result, there is no need to perform the experiments under different weather or light conditions. During the experiments, all drones had a constant altitude of 20 meters. For the sake of simplicity, Alta X was hovering with zero velocity. This was necessary since the antennas tend to point slightly toward the ground as Alta X moved forward. As a result, it was impossible to correct this beam misalignment without the elevation beamsteering functionality that was unavailable in this experiment.

The targets followed straight trajectories and were flying away from the radar platform at a certain speed to help discriminate against the ground clutter. In the meantime, the radar continuously recorded 7.5 seconds (equivalent to 25000 sweeps). After the measurements, the GPS and recorded IQ data were transferred to a PC to align them in time (based on their timestamps) and perform the post-processing with the help of MATLAB R2022a. Fig. 9 (a). presents Phantom's trajectory for the total duration of the recordings. Here, the geodetic coordinates provided by the onboard GPS sensors were transformed to east-north-up (ENU) Cartesian coordinates. The red arrows show the direction of the target's movement (e.g., away from the radar in this case). The intensity of the purple color illustrates the radar's antenna gain towards the respective angle. It can be observed that the antennas were almost perfectly aligned with the target in the azimuth plane.

Fig. 9 (b) shows a snapshot of the Range-Doppler map constructed through the integration of $N = 128$ sweeps that correspond to a time window of 38 milliseconds (from 2.81 to 2.848 seconds after the start of the recording). The reason for choosing $N = 128$ is to provide a decent processing gain without unnecessarily increasing the observation time (dwell time) towards this particular direction, given that the radar has to scan its beam in the angular domain quickly. A strong power peak associated with Phantom 4 returns is located at around 70 meters and 7 m/s in range and speed axis, respectively. The signature of the propellers due to the micro-Doppler effect is also clearly shown alongside the main peak. Regarding M600 Pro, a representative Range-Doppler snapshot of the

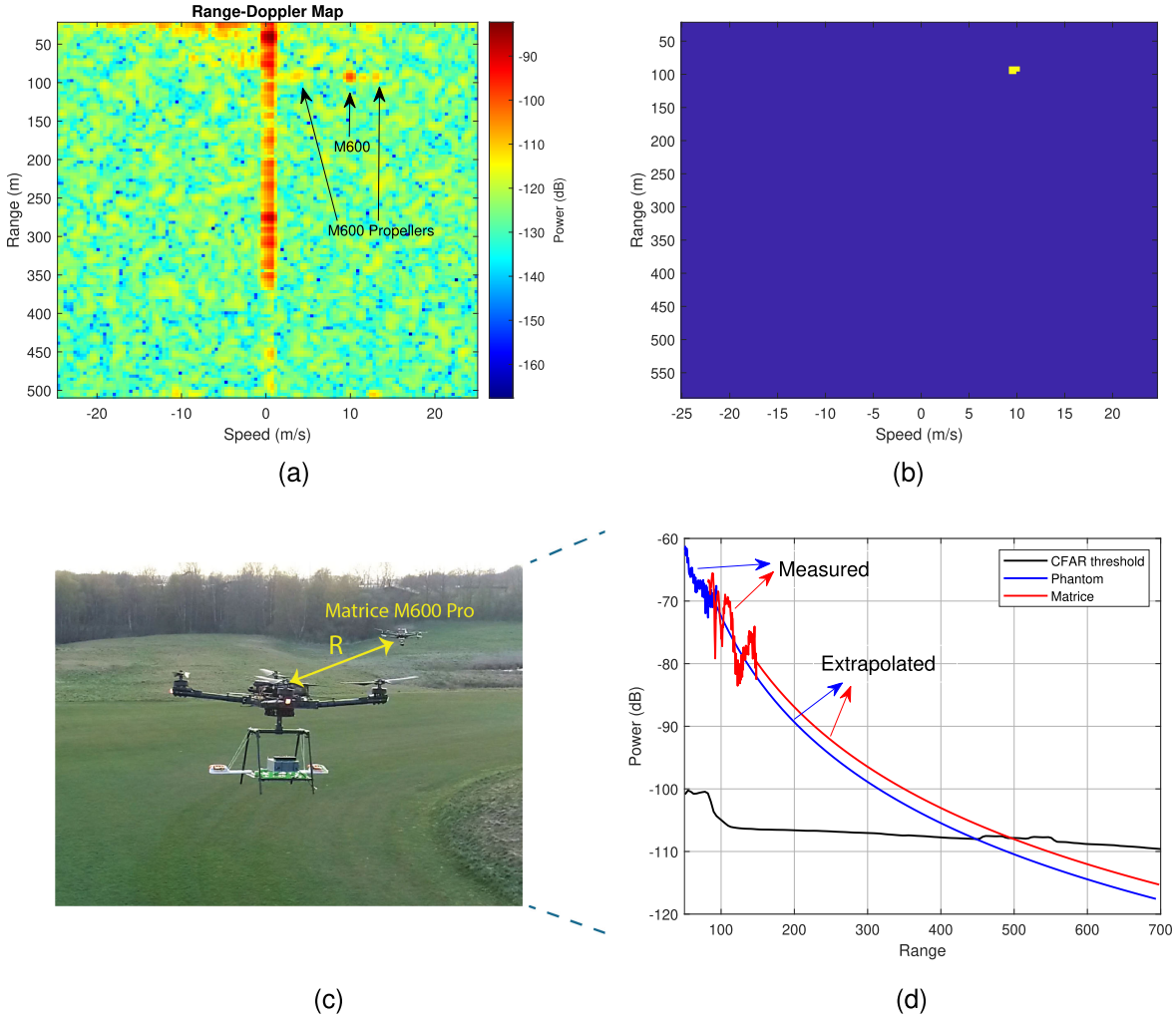

Fig. 10. (a) Range-doppler map constructed from M600 Pro measurements (b) Resulting image showing that M600 Pro is successfully detected after applying the CA-CFAR algorithm and MTI. (c) Photographs of the Alta X and M600 Pro drones during the experiments.(d) Measured and extrapolated the received power level of the target returns vs. Range. The CFAR threshold is also plotted to estimate the maximum detection range.

corresponding recordings is presented in Fig. 10 (a), where M600 Pro is found at around 100 meters, having a speed of approximately 10 m/s. As expected, the propeller signature here is stronger than Phantom's since there are two more propellers, they have a larger aperture, and are composed of a more reflective material (carbon fiber instead of plastic). The CFAR and MTI techniques are applied to distinguish the target return fully. The resulting image is presented in Fig. 10 (b), where M600 Pro is successfully isolated from the ground clutter and the surrounding noise.

To quantitatively estimate the maximum detection range (i.e., the range at which the target's echo is equal to the CFAR threshold) and assess the system performance, the measured values of the received power are extrapolated. This is achieved by considering the additional two-way, free-space path loss due to the increase in range. Hence, the received power for distances larger than the ones during the experiment (i.e., $d > d_0$) can be directly calculated as:

$$P_r(d) = P_r(d_0)\left(\frac{d_0}{d}\right)^4, \quad d > d_0 \tag{9}$$

where P_r is the received power, including the processing gain G_p due to integration of $N = 128$ sweeps, d_0 is the reference range at which the last measurement took place, and d is the range of interest. Here, d_0 is approximately 100 and 150 meters for Phantom 4 and M600 Pro, respectively.

For a fair estimation, the losses associated with the power dividers and cables must be considered. An attenuation factor denoted by α, which is equal to 4 when transformed to dB, is used to take these losses into account. Moreover, the attenuation caused by the high-pass filter used to preserve the dynamic range of the ADC has to be compensated as well. This is necessary since this filter exhibits higher attenuation (or equivalently lower gain) for targets at close distances (corresponding to low beat frequencies), as is the case for the experiments. By taking this into account, the calibrated received power $P_r'(d)$ level that does not include the cable, divider, and filter attenuation can be found by dividing with the attenuation factor a and the transfer function of the filter as follows:

$$P_r'(d) = \frac{P_r(d)}{\alpha H(d)}, \quad \forall d > 0 \tag{10}$$

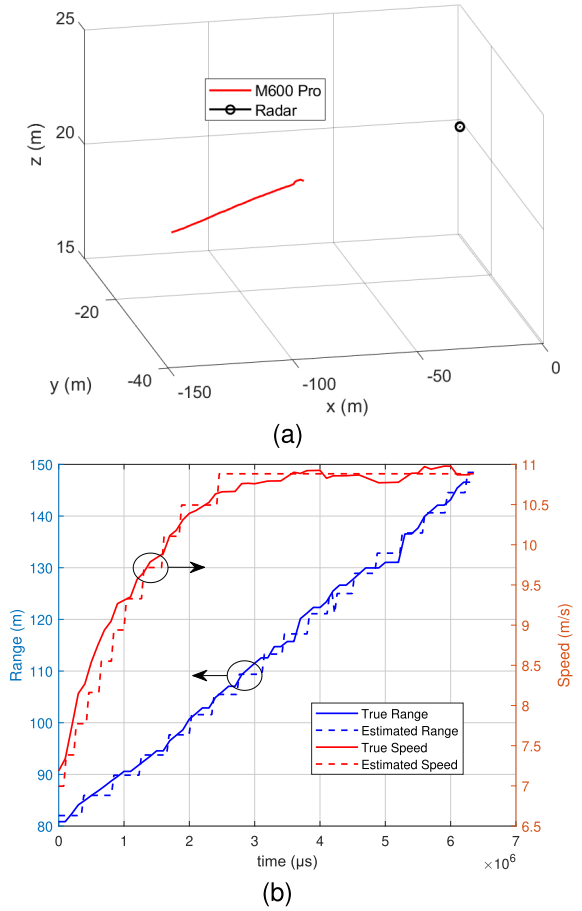

Fig. 11. (a) The GPS trajectory of the DJI M600 Pro drone during the experimental IQ recordings. (b) Comparison between the true (GPS) range and speed vs. the estimated (radar) data.

where $H(d)$ is the filter's transfer function with range d being used as the variable instead of the beat frequency given the transformation $d = \frac{cT_{sw}}{BW} f$.

A photograph of the Alta X and M600 Pro drones flying during the experiments and the measured and extrapolated results are shown in Fig. 10 (c). As shown, the measured received power for Phantom 4 is more stable regarding range, while M600 Pro's return power has more fluctuations. According to the extrapolation, the two drones can be successfully detected up to 440 meters and 500 meters away, respectively. It should be pointed out that this is a rough estimation, and the actual detection performance may vary depending on the propagation environment.

As far as accuracy is concerned, Fig. 11 (a) shows M600 Pro's trajectory during the experiments, and Fig. 11 (b) presents the corresponding true (GPS-retrieved) and estimated (radar) range and speed of M600 Pro relatively to the radar. An excellent agreement can be observed throughout the whole duration of the measurements, and thus the accuracy is validated. The exact values for the relative range and speed estimation errors do not exceed 3 m and 0.8 m/s, respectively.

V. Discussion

A. Target Classification

Target classification is crucial for the proposed radar system to distinguish drones from surrounding objects, birds, and other ground-based or flying vehicles. To achieve this, the most common method in the literature is exploiting the unique micro-Doppler signature of drones [39], [40], [41]. Combined with polarimetry techniques and machine learning algorithms, this method can yield excellent results. However, the applicability of this method to the proposed UAS-borne radar remains to be investigated. As shown, the radar-carrying drone's own propellers (e.g., Alta X in this case) have their own unique micro-Doppler signature, which will most likely interfere with the target's signature if they are closely spaced in the range-Doppler map. This is a serious concern that requires further investigation, and modifying the existing classification algorithms might be required to solve this. Furthermore, the reflections from the target drone propellers are typically 15-20 dB lower than the drone's main body. This means the micro-Doppler signature cannot be used for classification when the targets are far away. Hence, the classification range is anticipated to be less than half of the actual detection range.

B. Application Requirements

The cost, size, power consumption, and range specifications for the proposed UAS-borne radar will vary depending on the application. For example, the presented setup has a large form factor that is difficult to integrate into the low-cost, commercially available UAS platforms requiring onboard DAA capability. On the other hand, the more sophisticated and bigger UAS used for security applications might be able to accommodate a similar platform. For DAA applications, shorter detection ranges up to 100 meters can be considered, which could lead to design simplifications, reduction in payload size, and power consumption to enhance the flight endurance of drones for commercial applications, such as delivery, inspection, etc., to name a few. Meanwhile, the detection range for airspace surveillance applications can be further increased by adjusting some design parameters that improve the Signal-to-Noise Ratio (SNR), such as the processing gain (longer target observation time), antenna gain, or even transmitted power to effectively counter the threat of malicious drones to critical infrastructures and buildings.

C. Outlook

Despite the encouraging experimental results presented in this article, several challenges require further research and development efforts. For UAS-borne radars to be utilized by commercial drones of various sizes and form factors, developing and testing low-cost, small-size, and power-efficient solutions is essential. From a technical perspective, the unique characteristics of UASs, such as aerodynamic and mechanical factors, as well as operation at the VLL airspace, dictate even stricter requirements and exhibit more difficult engineering challenges for onboard drone radar platforms compared to their ground-based counterparts. For example, given that drones fly in 3D space, there is the need for accurate altitude estimation of targets (i.e., 4D radars [42]) and consequently deployment of large 2D antenna arrays that lead to increased size and signal processing complexity. In addition, the increased height and mobility require more sophisticated

clutter mitigation algorithms such as space-time adaptive processing (STAP) methods [43], [44], [45]. The relatively low RCS of drones compared to other vehicles (i.e., boats, cars, trucks) can impact detection range and increase the system's dynamic range specifications.

Regarding the processing techniques, the data processing models and algorithms developed and utilized in this paper are specifically designed to meet the requirements of the particular application examined here, with a special focus on the experiments and practical applicability of the methods. By exploiting the proposed system architecture and processing framework, the main goals of this paper, which are long-range drone detection with a UAS-borne sensor offering high accuracy, reliability and low complexity, have been achieved with great success. Therefore, further modifications to the proposed methods would most likely be incremental and expensive without yielding significant performance improvement. Therefore, the greatest future challenges of UAS-borne radars are primarily power, cost and size reduction rather than upgrading the signal processing models or similar technical concerns.

For this technology to be widely adopted while ensuring compatibility with other systems, a standardization framework is required to benchmark the performance levels necessary for UAS-borne radars, particularly for DAA applications in various environments. This could be similar to the case of automotive radars. The key performance indicators for UAS-borne radar quality could include maximum detection and classification range, the field of view, speed, angular resolution accuracy, and power consumption.

An interesting approach to reduce the cost and mitigate interference between radars is the deployment of UAS radar networks, similar to those examined in [25] and [46]. In this scenario, several bigger drones are equipped with long-range advanced radar sensors to share their detection and tracking data with other drones over low-latency 5G and beyond and 6G networks. Several dedicated UAS platforms compatible with airborne radars could be developed for this purpose. At the same time, the smaller drones can still potentially carry low-cost, short-range radars for additional safety.

Unarguably, the proposed UAS-borne radar systems have many similarities with automotive, aerospace, and other vehicular radars. However, it also exhibits unique characteristics that differentiate it from different radar types. In general, it is concluded that further research and development are required to comprehend the opportunities and limitations of UAS-borne radars fully.

VI. Conclusion

A complete UAS-borne radar system capable of detecting drones is presented in this article. Initially, the theoretical principles and the practical design and implementation of the UAS-borne radar platform are presented and described in detail. Subsequently, a measurement campaign is conducted to evaluate the performance and examine the limitations of the proposed method. The experimental results exhibit the efficacy of the UAS-borne radar system by detecting a DJI Phantom 4 and a DJI Matrice 600 Pro at a maximum range of 440 and 500 meters, respectively. The detection range can be adjusted depending on application requirements, drone types, and cost. The proposed platform is extremely useful for several applications, such as airspace surveillance, traffic management, intelligent transportation systems, security and privacy enhancement against malicious drones, and detect-and-avoid (DAA) systems for autonomous UASs. The need for further research and development is highlighted while future challenges and research directions are discussed.

Acknowledgment

The authors would like to thank Anders Gregersen for providing drone piloting support and El & Svæv, Silkeborg, Denmark, for providing drone flight facilities to execute the experiments.

References

[1] *European Drones Outlook Study: Unlocking the Value for Europe*, Undertaking, SESAR Joint, Publications Office Eur. Union, Brussels, Belgium, 2017.

[2] *Unmanned Aircraft Systems Traffic Management (UTM)—A Common Framework With Core Principles for Global Harmonization*, International Civil Aviation Organization (ICAO), Montreal, QC, Canada, 2020.

[3] P. Kopardekar, "Unmanned aircraft system traffic management (UTM) concept of operations," AIAA Aviation Aeronaut. Forum, Washington, DC, USA, Tech. Rep., ARC-E-DAA-TN32838. 2016.

[4] C. Barrado et al., "U-space concept of operations: A key enabler for opening airspace to emerging low-altitude operations," *Aerospace*, vol. 7, no. 3, p. 24, Mar. 2020.

[5] J. L. Rios, A. S. Aweiss, J. Jung, J. Homola, M. Johnson, and R. Johnson, "Flight demonstration of unmanned aircraft system (UAS) traffic management (UTM) at technical capability level 4," in *Proc. AIAA AVIATION FORUM*, Jun. 2020, p. 2851.

[6] H. Liu, X. Li, M. Fan, G. Wu, W. Pedrycz, and P. N. Suganthan, "An autonomous path planning method for unmanned aerial vehicle based on a tangent intersection and target guidance strategy," *IEEE Trans. Intell. Transp. Syst.*, vol. 23, no. 4, pp. 3061–3073, Apr. 2022, doi: 10.1109/TITS.2020.3030444.

[7] I. Guvenc, F. Koohifar, S. Singh, M. L. Sichitiu, and D. Matolak, "Detection, tracking, and interdiction for amateur drones," *IEEE Commun. Mag.*, vol. 56, no. 4, pp. 75–81, Apr. 2018, doi: 10.1109/MCOM.2018.1700455.

[8] S. Dogru and L. Marques, "Drone detection using sparse LiDAR measurements," *IEEE Robot. Autom. Lett.*, vol. 7, no. 2, pp. 3062–3069, Apr. 2022, doi: 10.1109/LRA.2022.3145498.

[9] M. Hammer, M. Hebel, M. Laurenzis, and M. Arens, "LiDAR-based detection and tracking of small UAVs," *Emerg. Imag. Sens. Technol. Secur. Defence III, Unmanned Sensors, Syst., Countermeasures*, vol. 10799, pp. 177–185, Oct. 2018.

[10] Y. Miao, Y. Tang, B. A. Alzahrani, A. Barnawi, T. Alafif, and L. Hu, "Airborne LiDAR assisted obstacle recognition and intrusion detection towards unmanned aerial vehicle: Architecture, modeling and evaluation," *IEEE Trans. Intell. Transp. Syst.*, vol. 22, no. 7, pp. 4531–4540, Jul. 2021, doi: 10.1109/TITS.2020.3023189.

[11] M. U. de Haag, C. G. Bartone, and M. S. Braasch, "Flight-test evaluation of small form-factor LiDAR and radar sensors for sUAS detect-and-avoid applications," in *Proc. IEEE/AIAA 35th Digit. Avionics Syst. Conf. (DASC)*, Sep. 2016, pp. 1–11, doi: 10.1109/DASC.2016.7778108.

[12] J. Zhao, J. Zhang, D. Li, and D. Wang, "Vision-based anti-UAV detection and tracking," *IEEE Trans. Intell. Transp. Syst.*, vol. 23, no. 12, pp. 25323–25334, Dec. 2022, doi: 10.1109/TITS.2022.3177627.

[13] G. Laurito, B. Fraser, and K. Rosser, "Airborne localisation of small UAS using visual detection: A field experiment," in *Proc. IEEE Symp. Ser. Comput. Intell. (SSCI)*, Dec. 2020, pp. 1435–1443, doi: 10.1109/SSCI47803.2020.9308605.

[14] A. Carrio, J. Tordesillas, S. Vemprala, S. Saripalli, P. Campoy, and J. P. How, "Onboard detection and localization of drones using depth maps," *IEEE Access*, vol. 8, pp. 30480–30490, 2020, doi: 10.1109/ACCESS.2020.2971938.

[15] Z. Shi, X. Chang, C. Yang, Z. Wu, and J. Wu, "An acoustic-based surveillance system for amateur drones detection and localization," *IEEE Trans. Veh. Technol.*, vol. 69, no. 3, pp. 2731–2739, Mar. 2020, doi: 10.1109/TVT.2020.2964110.

[16] M. Z. Anwar, Z. Kaleem, and A. Jamalipour, "Machine learning inspired sound-based amateur drone detection for public safety applications," *IEEE Trans. Veh. Technol.*, vol. 68, no. 3, pp. 2526–2534, Mar. 2019, doi: 10.1109/TVT.2019.2893615.

[17] H. Fu, S. Abeywickrama, L. Zhang, and C. Yuen, "Low-complexity portable passive drone surveillance via SDR-based signal processing," *IEEE Commun. Mag.*, vol. 56, no. 4, pp. 112–118, Apr. 2018, doi: 10.1109/MCOM.2018.1700424.

[18] S. Basak, S. Rajendran, S. Pollin, and B. Scheers, "Combined RF-based drone detection and classification," *IEEE Trans. Cognit. Commun. Netw.*, vol. 8, no. 1, pp. 111–120, Mar. 2022, doi: 10.1109/TCCN.2021.3099114.

[19] D.-H. Shin, D.-H. Jung, D.-C. Kim, J.-W. Ham, and S.-O. Park, "A distributed FMCW radar system based on fiber-optic links for small drone detection," *IEEE Trans. Instrum. Meas.*, vol. 66, no. 2, pp. 340–347, Feb. 2017, doi: 10.1109/TIM.2016.2626038.

[20] F. Hoffmann, M. Ritchie, F. Fioranelli, A. Charlish, and H. Griffiths, "Micro-Doppler based detection and tracking of UAVs with multistatic radar," in *Proc. IEEE Radar Conf. (RadarConf)*, May 2016, pp. 1–6.

[21] D. Solomitckii, M. Gapeyenko, V. Semkin, S. Andreev, and Y. Koucheryavy, "Technologies for efficient amateur drone detection in 5G millimeter-wave cellular infrastructure," *IEEE Commun. Mag.*, vol. 56, no. 1, pp. 43–50, Jan. 2018, doi: 10.1109/MCOM.2017.1700450.

[22] A. K. Singh and Y.-H. Kim, "Automatic measurement of blade length and rotation rate of drone using W-band micro-Doppler radar," *IEEE Sensors J.*, vol. 18, no. 5, pp. 1895–1902, Mar. 2018, doi: 10.1109/JSEN.2017.2785335.

[23] Y. Rong, R. Gutierrez, K. V. Mishra, and D. W. Bliss, "Noncontact vital sign detection with UAV-borne radars: An overview of recent advances," *IEEE Veh. Technol. Mag.*, vol. 16, no. 3, pp. 118–128, Sep. 2021, doi: 10.1109/MVT.2021.3086442.

[24] Y. A. Nijsure, G. Kaddoum, N. K. Mallat, G. Gagnon, and F. Gagnon, "Cognitive chaotic UWB-MIMO detect-avoid radar for autonomous UAV navigation," *IEEE Trans. Intell. Transp. Syst.*, vol. 17, no. 11, pp. 3121–3131, Nov. 2016, doi: 10.1109/TITS.2016.2539002.

[25] A. Guerra, D. Dardari, and P. M. Djuric, "Dynamic radar networks of UAVs: A tutorial overview and tracking performance comparison with terrestrial radar networks," *IEEE Veh. Technol. Mag.*, vol. 15, no. 2, pp. 113–120, Jun. 2020, doi: 10.1109/MVT.2020.2979698.

[26] A. Moses, M. J. Rutherford, M. Kontitsis, and K. P. Valavanis, "UAV-borne X-band radar for collision avoidance," *Robotica*, vol. 32, no. 1, pp. 97–114, 2014.

[27] S. Dogru and L. Marques, "Pursuing drones with drones using millimeter wave radar," *IEEE Robot. Autom. Lett.*, vol. 5, no. 3, pp. 4156–4163, Jul. 2020, doi: 10.1109/LRA.2020.2990605.

[28] M. Kronauge and H. Rohling, "New chirp sequence radar waveform," *IEEE Trans. Aerosp. Electron. Syst.*, vol. 50, no. 4, pp. 2870–2877, Oct. 2014.

[29] H. M. Finn and R. S. Johnson, "Adaptive detection mode with threshold control as a function of spatially sampled clutter-level estimates," *RCA Rev.*, vol. 29, pp. 414–464, Sep. 1968.

[30] M. Ash, M. Ritchie, and K. Chetty, "On the application of digital moving target indication techniques to short-range FMCW radar data," *IEEE Sensors J.*, vol. 18, no. 10, pp. 4167–4175, May 2018, doi: 10.1109/JSEN.2018.2823588.

[31] Y. Wang, Y. Peng, and Z. Bao, "Space-time adaptive processing for airborne radar with various array orientations," *IEE Proc.-Radar Sonar Navigat.*, vol. 144, no. 6, pp. 330–340, Dec. 1997.

[32] S. Rahman and D. A. Robertson, "In-flight RCS measurements of drones and birds at K-band and W-band," *IET Radar, Sonar Navigat.*, vol. 13, no. 2, pp. 300–309, 2018.

[33] P. Sedivy and O. Nemec. *Drone RCS Statistical Behaviour*. Accessed: Nov. 5, 2022. [Online]. Available: https://www.sto.nato.int/publications/%201134%20STO%20Meeting%20Proceedings/STO-MP-MSG-SET-183/MP-MSG1135%20SET-183-04.pdf

[34] S. Ayhan, S. Scherr, A. Bhutani, B. Fischbach, M. Pauli, and T. Zwick, "Impact of frequency ramp nonlinearity, phase noise, and SNR on FMCW radar accuracy," *IEEE Trans. Microw. Theory Techn.*, vol. 64, no. 10, pp. 3290–3301, Aug. 2016.

[35] D. A. Shnidman, "Expanded Swerling target models," *IEEE Trans. Aerosp. Electron. Syst.*, vol. 39, no. 3, pp. 1059–1069, Jul. 2003.

[36] *Alta X—Freefly*. Accessed: Jul. 4, 2022. [Online]. Available: https://freeflysystems.com/alta-x

[37] J. Park, S. Park, D.-H. Kim, and S.-O. Park, "Leakage mitigation in heterodyne FMCW radar for small drone detection with stationary point concentration technique," *IEEE Trans. Microw. Theory Techn.*, vol. 67, no. 3, pp. 1221–1232, Mar. 2019, doi: 10.1109/TMTT.2018.2889045.

[38] A. Melzer, A. Onic, F. Starzer, and M. Huemer, "Short-range leakage cancelation in FMCW radar transceivers using an artificial on-chip target," *IEEE J. Sel. Topics Signal Process.*, vol. 9, no. 8, pp. 1650–1660, Dec. 2015, doi: 10.1109/JSTSP.2015.2465298.

[39] S. Rahman and D. A. Robertson, "Radar micro-Doppler signatures of drones and birds at K-band and W-band," *Sci. Rep.*, vol. 8, no. 1, p. 17396, Nov. 2018.

[40] B. K. Kim, H.-S. Kang, and S.-O. Park, "Experimental analysis of small drone polarimetry based on micro-Doppler signature," *IEEE Geosci. Remote Sens. Lett.*, vol. 14, no. 10, pp. 1670–1674, Oct. 2017, doi: 10.1109/LGRS.2017.2727824.

[41] C. J. Li and H. Ling, "An investigation on the radar signatures of small consumer drones," *IEEE Antennas Wireless Propag. Lett.*, vol. 16, pp. 649–652, 2016, doi: 10.1109/LAWP.2016.2594766.

[42] S. Sun and Y. D. Zhang, "4D automotive radar sensing for autonomous vehicles: A sparsity-oriented approach," *IEEE J. Sel. Topics Signal Process.*, vol. 15, no. 4, pp. 879–891, Jun. 2021, doi: 10.1109/JSTSP.2021.3079626.

[43] Y. Wang and S. Zhu, "Range ambiguous clutter suppression for FDA-MIMO forward looking airborne radar based on main lobe correction," *IEEE Trans. Veh. Technol.*, vol. 70, no. 3, pp. 2032–2046, Mar. 2021, doi: 10.1109/TVT.2021.3057436.

[44] X. He, G. Liao, S. Zhu, J. Xu, and J. Zhu, "Range ambiguous clutter suppression approach with elevation time diverse array," *IEEE Trans. Aerosp. Electron. Syst.*, vol. 58, no. 1, pp. 359–373, Feb. 2022, doi: 10.1109/TAES.2021.3101786.

[45] X. Yang, Y. Sun, T. Zeng, T. Long, and T. K. Sarkar, "Fast STAP method based on PAST with sparse constraint for airborne phased array radar," *IEEE Trans. Signal Process.*, vol. 64, no. 17, pp. 4550–4561, Sep. 2016, doi: 10.1109/TSP.2016.2569471.

[46] A. Guerra, D. Dardari, and P. M. Djurić, "Dynamic radar network of UAVs: A joint navigation and tracking approach," *IEEE Access*, vol. 8, pp. 116454–116469, 2020, doi: 10.1109/ACCESS.2020.3001393.

Christos Milias (Student Member, IEEE) received the M.Sc. degree in electrical and computer engineering from the Aristotle University of Thessaloniki, Greece, in 2020. He is currently pursuing the joint Ph.D. (Industrial) degree in collaboration with MyDefence A/S, Nørresundby, Denmark, and the Department of Business and Technology (BTECH), Aarhus University, Denmark, within the framework of the H2020 European project MOTOR5G. His research interests include antennas and propagation, metamaterials, UAVs, and radar systems.

Rasmus B. Andersen received the M.S. degree in advanced radio frequency design from Aalborg University, Denmark, in 2001. Since 2001, he has been working in the telecommunication industry implementing RF systems from the antenna to software-defined baseband. From 2011 to 2016, he worked as the Project Manager within organic photovoltaics with Mekoprint and joined MyDefence in 2016 as a Senior Hardware Engineer focusing on drone RF sensors, electronic countermeasures, and radar sensing. He has headed projects in the fields of product development, commercial-academic collaboration, MIL-STD, medical approvals, process control, and application engineering.

Bilal Muhammad received the Ph.D. degree in telecommunication engineering from the University of Rome "Tor Vergata," Italy. Currently, he is working as an Assistant Professor with the Department of Business Development and Technology (BTECH), Aarhus University, Denmark. His research interests include UAV wireless communication for 5G and beyond, GNSS integrity and accuracy for UAV, and unmanned traffic management (UTM) systems and services.

Jes T. B. Kristensen received the M.Sc. degree in electrical engineering from Aalborg University, Denmark, in 2008, with a specialization in applied signal processing and implementation. From 2008 to 2014, he worked with Rohde & Schwarz (TCDK—Aalborg/Denmark and Munich) as a FPGA and a Baseband Developer for WCDMA L1 testing for the CRTU and CMW500 products. Additionally, he worked as a technical consultant for starting and facilitating the TD-SCDMA development with R&S China and the Beijing universities. Since 2014, he has been working with MyDefence (http://mydefence.dk), Denmark, as a Signal Processing Engineer and a General Architect for C-UAV sensors.

Pavlos I. Lazaridis (Senior Member, IEEE) received the M.Eng. degree from the Aristotle University of Thessaloniki, Greece, in 1990, the M.Sc. degree from Paris 6, France, in 1992, and the joint Ph.D. degree from ENST and Paris 6, Paris, in 1996. In 1997, he became the Head of the Antennas and Propagation Laboratory, TDF-C2R. From 1998 to 2002, he was with EPO as a Senior Patent Examiner. From 2002 to 2014, he was with ATEI Thessaloniki, Greece, and Brunel University, West London. He is currently a Professor with the University of Huddersfield, U.K. He has more than 150 publications and patents. He is also a member of the IET and SM-URSI.

Zaharias D. Zaharis (Senior Member, IEEE) received the M.Sc. degree in electronics and in electrical and computer engineering and the Ph.D. degree in antennas and propagation modeling for mobile communications. He is currently a physicist. His current research interests include designing and optimizing antennas and microwave circuits, signal processing on smart antennas, developing evolutionary optimization algorithms and neural networks, and the evolution of 6G infrastructure. Recently, he was the elected Chair of the Electron Devices/Microwave Theory and Techniques/Antennas and Propagation Joint Chapter of the IEEE Greece Section. He is currently serving as an Associate Editor for IEEE ACCESS.

Albena Mihovska (Member, IEEE) received the Ph.D. degree in mobile communications from Aalborg University, Denmark. She has been an Associate Professor with the Department of Business Development and Technology, Aarhus University, Denmark, since 2017, where she is leading the research activities of the 6G Knowledge Laboratory with a focus on 6G connectivity and enabling technologies (e.g., artificial intelligence) and advanced services and applications, such as augmented and extended reality (AR, XR), high-fidelity and real-time mobile hologram, and digital twins. She has more than 150 scientific publications. She is currently a senior research and an academician professional.

Dan D. S. Hermansen received the M.Sc. degree in RF engineering and CMOS IC design from Aalborg University, Denmark, in 2005. He has worked in the telecommunication industry for over 20 years on RF-related systems and technologies. In 2013, he co-founded MyDefence, which works with security-related applications like anti-drone equipment, including RF sensors, RF jammers, radars, and data fusion. MyDefence has completed numerous research projects within the EU (e.g., H2020) and Danish Defence and Innovation Fund Denmark research programmes, where he has headed the projects.